

Orientation and Motion of Tetrahydrofuran in Graphite Intercalation Compounds: Proton NMR Studies of Cs(THF)_{1.3}C₂₄ and K(THF)_{2.5}C₂₄

C. Schmidt,[†] M. E. Rosen,[‡] D. F. Caplan, and A. Pines*

Materials and Chemical Sciences Division, Lawrence Berkeley Laboratory, 1 Cyclotron Road, Berkeley, California 94720, and Department of Chemistry, University of California, Berkeley, California 94720

M. F. Quinton

Laboratoire de Physique Quantique, CNRS-URA 1428, E.S.P.C.I., 10, rue Vauquelin, F-75231 Paris Cédex 05, France

Received: September 21, 1994; In Final Form: March 9, 1995[®]

The orientation and motion of tetrahydrofuran (THF) in the ternary graphite intercalation compounds Cs(THF)_{1.3}C₂₄ and K(THF)_{2.5}C₂₄ have been studied by proton NMR. Simulations of the NMR spectra indicate that the THF molecules in Cs(THF)_{1.3}C₂₄ have their mean planes oriented parallel to the layers of the host lattice, while the THF molecules in K(THF)_{2.5}C₂₄ have their mean planes oriented at an angle between 50° and 75° from the graphite layers. The proton NMR spectra of both compounds show evidence that the THF molecules rotate about the normal to the graphite layers and confirm X-ray diffraction studies showing a degree of orientational disorder in the samples, corresponding to a mosaic spread in the graphite layer orientation. The conformation of the intercalated THF was studied by simulating the experimental NMR spectra using models for the conformational motion of THF. Simulations indicate that the conformation of intercalated THF is different than gas or liquid phase THF, which has been found to have a ring puckering amplitude of 0.38–0.44 Å and to undergo nearly free pseudorotation through a series of conformations. Best agreement between simulated and experimental NMR spectra of Cs(THF)_{1.3}C₂₄ was obtained with THF interconverting between two conformations of C_s symmetry and a puckering amplitude of 0.30 Å. Free or slightly hindered pseudorotation of THF (observed in liquid or gaseous THF) in this compound produces simulated spectra that differ significantly from the experimental spectra. Simulated proton NMR spectra of K(THF)_{2.5}C₂₄ using conformations of C_s symmetry or free or slightly hindered pseudorotation of THF do not fit the experimental spectra sufficiently well to allow distinction between the conformational motions or to exclude other possible motions.

1. Introduction

Since the early days of NMR spectroscopy, line shape analysis of NMR spectra has made possible the investigation of molecular motion. NMR line shape provides direct evidence of nuclear couplings that depend on the relative positions of the nuclei. When molecules undergo rapid motion, the coordinates of their nuclei become time-dependent, and the nuclear couplings are time-averaged. NMR spectra of such molecules typically contain lines that are narrower and modified in shape relative to those observed in the absence of rapid motion.¹ In the presence of rapid, isotropic motion, as occurs in the liquid state, position- and orientation-dependent nuclear spin interactions are averaged to zero, allowing observation of only the isotropic nuclear spin Hamiltonian. In the presence of anisotropic motion, the position- and orientation-dependent nuclear spin interactions are incompletely averaged, leaving a residual anisotropic contribution to the nuclear spin Hamiltonian. In a sample where all the molecules undergo the same types of anisotropic molecular motion, the NMR spectrum can display well-resolved structure that is directly related to the conformation and orientation of the molecule. This is the case, for example, for organic molecules dissolved in liquid crystals and

has resulted in the widespread use of NMR in liquid crystal solvents as a method for molecular structure determination.²

Anisotropic motions also occur in solid state compounds, in particular for molecules that are adsorbed, as in zeolites, or weakly bound to host lattices, as in layered compounds. Graphite intercalation compounds (GICs) are one type of layered compound where the intercalated species generally undergo rapid motion at room temperature.^{3–5} These motions have been shown to be strongly anisotropic due to the constrained environment imposed by the host graphite layers both in powder GIC samples^{6,7} and in highly oriented pyrolytic graphite (HOPG) GIC samples (Figure 1), where the presence of a well-defined c axis throughout the sample has facilitated the observation that the preferential reorientation axis for the intercalated species is the c axis, perpendicular to the graphite layers.^{8,9}

Ternary GICs prepared by sequential intercalation of tetrahydrofuran (THF) into binary alkali metal GICs (Figure 2) are of special interest for several reasons. First, different types of anisotropic motion of THF can occur in the intercalated layer, depending on the nature of the alkali atom, the concentration of THF, and the temperature.^{10–13} Second, in some cases, the proton NMR spectrum of intercalated THF displays a very well-resolved, complex structure,¹⁴ possibly allowing the extraction of precise information about the motion of THF in these compounds. Finally, it is of interest to determine whether the THF molecules in the GICs undergo pseudorotation, a large-amplitude ring vibration common to five-membered-ring mol-

[†] Permanent address: Institut für Makromolekulare Chemie, Universität Freiburg, Stefan-Meier-Str. 31, D-79104 Freiburg, Germany.

[‡] Permanent address: NMR Facility, Department of Chemistry, University of Minnesota, Minneapolis, MN 55455.

[®] Abstract published in *Advance ACS Abstracts*, May 1, 1995.

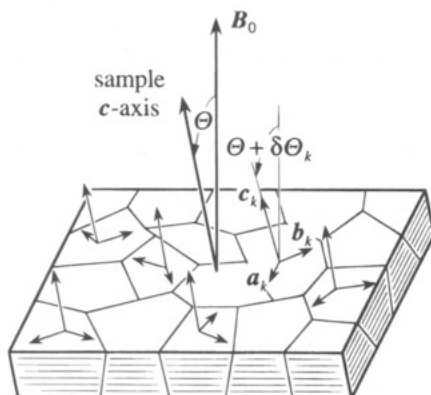


Figure 1. Schematic representation of a highly oriented pyrolytic graphite (HOPG) sample. The orientational dispersion of the crystallite c_k axis about the sample c axis is very small, but the a_k and b_k axes are distributed randomly.

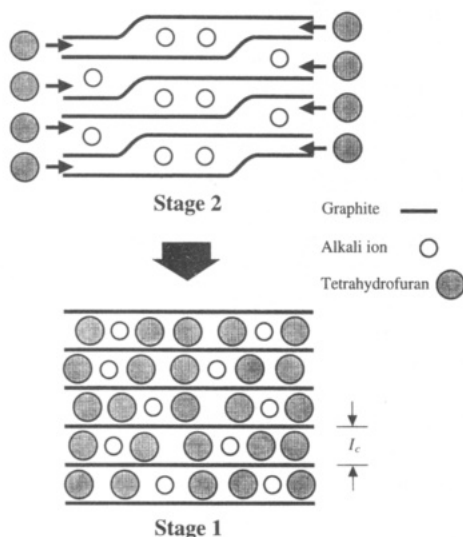


Figure 2. Pleated layer model for intercalation of THF into the binary stage 2 alkali GIC to form the stage 1 ternary alkali/THF GIC.

olecules in the gas or liquid phase that is observed in gaseous and liquid THF.^{15–18}

We present here an analysis of the proton NMR spectra of $\text{Cs}(\text{THF})_{1.3}\text{C}_{24}$ and $\text{K}(\text{THF})_{2.5}\text{C}_{24}$ compounds prepared from HOPG to determine the nature of the motions of the THF molecules in these compounds.

2. Experimental Section

The samples of $\text{Cs}(\text{THF})_{1.3}\text{C}_{24}$ and $\text{K}(\text{THF})_{2.5}\text{C}_{24}$ were prepared by sequential intercalation of THF into the binary alkali metal GIC using the method described previously for ex-HOPG samples.^{11,14} The amount of K or Cs was estimated from the X-ray (00 l) diffraction pattern of the host binary GIC. The THF/ C_{24} molecular ratio was obtained from the measurement of THF consumption during intercalation, leading to ternary samples of composition $\text{K}_x(\text{THF})_{2.5}\text{C}_{24}$ and $\text{Cs}_x(\text{THF})_{1.3}\text{C}_{24}$ with $x = 1.0 \pm 0.15$. The Cs/THF graphite sample contains less intercalated THF than is usually found in saturated Cs/THF GICs with the composition $\text{Cs}_x(\text{THF})_{1.6}\text{C}_{24}$,^{12,14,19} and the X-ray (00 l) profile of the sample, which gives information about the periodic sequence of intercalant and graphite layers, shows that the sample is not a pure phase. For the major phase (>90%), however, the spacing between the two nearest intercalated layers is $I_c = 7.06 \pm 0.01 \text{ \AA}$, very close to the value found for the saturated Cs/THF GIC compound.¹² Moreover, with the exception of the broad peak in the center of the spectrum that can be

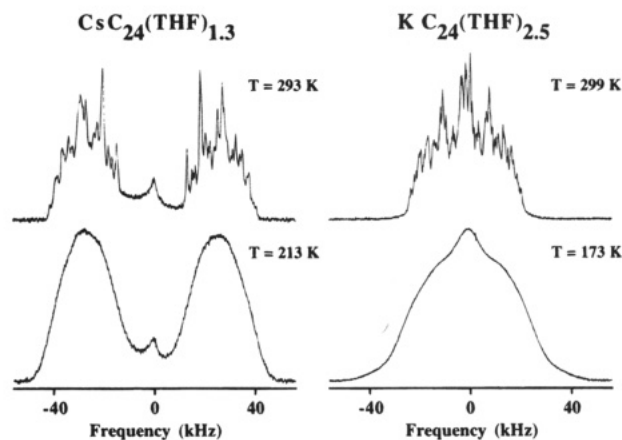


Figure 3. Experimental ^1H NMR spectra of $\text{Cs}(\text{THF})_{1.3}\text{C}_{24}$ and $\text{K}(\text{THF})_{2.5}\text{C}_{24}$ with the graphite layers perpendicular to the external magnetic field. The transition from immobile THF at low temperature to mobile THF at room temperature is clearly evident from the changes in line shape in the spectra.

attributed to THF molecules in the minor phase, the proton NMR spectrum of this sample is the same as that of a saturated Cs/THF GIC sample with the higher THF/ C_{24} ratio of 1.6.¹⁴

NMR experiments were performed on a Bruker CXP-100 spectrometer operating at a proton frequency of 100 MHz. The probe was a high-power, variable-temperature Bruker probe with the solenoid coil oriented perpendicular to the static magnetic field \mathbf{B}_0 . The sample orientation relative to the magnetic field was varied by rotating the sample inside the coil and was adjusted to the desired angle by eye. The error in the angle Θ between the sample c axis (perpendicular to the graphite layers) and the external magnetic field was estimated to be $\pm 2.5^\circ$ at $\Theta = 0^\circ$ and 90° and $\pm 10^\circ$ at intermediate angles.

The proton NMR spectra were obtained using a simple one-pulse sequence (θ pulse—dead time—acquire FID—recycle delay) _{N} . The strength of the radio-frequency field was about 190 kHz, as deduced from the $\pi/2$ pulse length of 1.3 μs . To obtain spectra free of probe background signal, two FIDs were acquired using different recycle delays, and the Fourier transform was performed on the difference of the two FIDs. By elimination of the background signal in this manner, it was possible to reduce the dead time to 1 μs , minimizing distortion of the spectra due to the loss of the beginning of the FID.²⁰

3. Proton NMR Spectra

3.1. Temperature Dependence. The proton NMR spectra of the Cs/THF and K/THF GICs are shown in Figure 3 at temperatures above and below a phase transition. The spectra of both compounds are broad and featureless at low temperature, since the THF molecules are almost immobile. As the temperature increases, so does the mobility of the THF, resulting in sharper spectral features due to averaging of intermolecular dipole couplings. It can also be seen that the line shapes in the spectra of the two samples are dramatically different. The Cs/THF GIC spectrum is a doublet spread over about 80 kHz, with a splitting of about 55 kHz. No such doublet is observed with the K/THF GIC sample, and the spectrum is only about 45 kHz wide. This difference can be understood if it is assumed that the line shape is mainly determined by the dipolar couplings between pairs of protons on the same THF molecule. The strength of this coupling is proportional to $\langle (3 \cos^2 \Theta_{ij} - 1) / r_{ij}^3 \rangle$ where Θ_{ij} is the angle between the external magnetic field \mathbf{B}_0 and the proton—proton internuclear vector \mathbf{r}_{ij} , and the angular brackets indicate an average over all molecular motions. A THF molecule is an eight-proton system or, alternatively, a four-

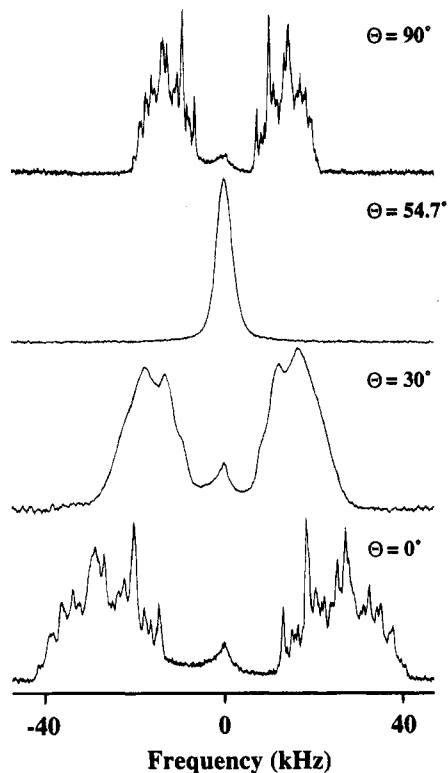


Figure 4. Experimental ^1H NMR spectra of $\text{Cs}(\text{THF})_{1.3}\text{C}_{24}$ for different angles Θ between the normal to the graphite layers and the external magnetic field. The overall width of the features in the spectra scale as $(3 \cos^2 \Theta - 1)$, indicating rotation of THF about an axis perpendicular to the graphite layers.

proton-pair system composed of CH_2 proton pairs. With the GIC sample at the orientation $\Theta = 0^\circ$, the internuclear vector, Θ_{ij} , between protons in a CH_2 pair is approximately the angle between \mathbf{r}_{ij} and the sample c axis. If the mean planes of the THF molecules are parallel to the graphite planes, the *intrapair* internuclear vectors are parallel to the c axis, and the corresponding averaged dipolar couplings are much larger than the *interpair* couplings, giving an expected line shape of a broad doublet. If the mean planes of THF molecules are significantly tilted with respect to the graphite planes, the intra- and interpair couplings have comparable values and the doublet collapses to a singlet.

From this qualitative analysis, we can conclude that in the Cs/THF GIC the mean planes of the THF molecules are nearly parallel to the graphite layers, while in the K/THF compound the mean planes of the THF molecules are tilted relative to the graphite layers.

3.2. Orientation Dependence at Room Temperature. The proton NMR spectra of $\text{Cs}(\text{THF})_{1.3}\text{C}_{24}$ and $\text{K}(\text{THF})_{2.5}\text{C}_{24}$ are shown in Figures 4 and 5 at a series of orientations, Θ , with respect to the applied magnetic field. The overall width of the spectra show a characteristic $(3 \cos^2 \Theta - 1)$ dependence with the Cs/THF compound showing this dependence for both the splitting of the doublet and the width of each half of the doublet. The spectra also demonstrate a modification of the line shape and a noticeable loss of resolution when the sample orientation deviates from 0° or 90° .

As shown in the Appendix, this $(3 \cos^2 \Theta - 1)$ orientational dependence of the line width in a two-dimensional polycrystalline sample implies that the sample c axis is a symmetry axis for the THF anisotropic motion. As a consequence, the small mosaic distribution of the crystallites causes a small dispersion of dipolar coupling constants that is roughly proportional to $\sin 2\Theta$, resulting in the observed loss of resolution in the spectra

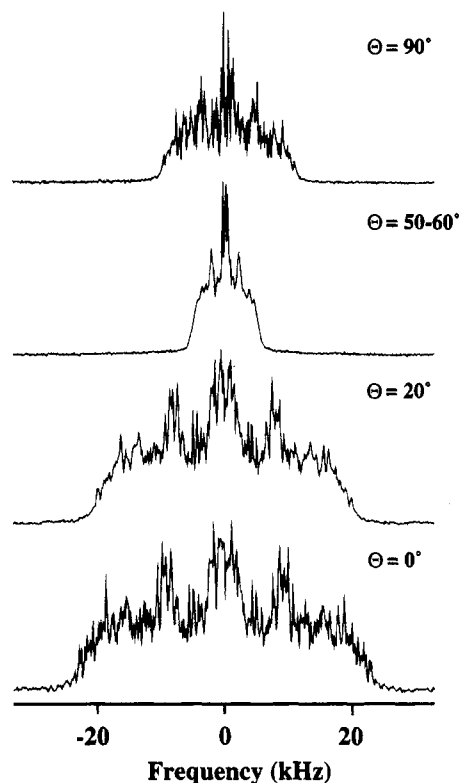


Figure 5. Experimental ^1H NMR spectra of $\text{K}(\text{THF})_{2.5}\text{C}_{24}$ for several angles Θ , defined in Figure 4. Like in Figure 4, the overall width of the spectra scales as $(3 \cos^2 \Theta - 1)$, giving evidence of rotation of THF about an axis perpendicular to the graphite layers.

at values of Θ different from 0° and 90° . Though strongly reduced at $\Theta = 0^\circ$ and 90° , the effect of the spread in crystallite c axis alignment is discernible. At these orientations, individual lines in the spectra of the Cs/THF compound appear to be broader than those in the spectra of the K/THF sample, as expected by comparing the crystallite c axis mosaic distribution in both compounds (Figure 6).

4. Simulation of the NMR Spectra

4.1. Hamiltonian. The shape of the proton spectra of $\text{Cs}(\text{THF})_{1.3}\text{C}_{24}$ and $\text{K}(\text{THF})_{2.5}\text{C}_{24}$ is mainly determined by the magnetic dipole-dipole coupling between protons on the intercalated THF. The dipolar Hamiltonian, \mathcal{H}_D , is given by the sum over all spin pairs i, j of the pairwise dipole coupling:

$$\mathcal{H}_D = \sum_i \sum_{j>i} \mathcal{H}_D^{ij} \quad (1)$$

The dipole coupling between two identical spins- $1/2$, \mathcal{H}_D^{ij} , is given by

$$\mathcal{H}_D^{ij} = -\frac{\gamma^2 \hbar}{2\pi} \frac{1}{2r_{ij}^3} (3 \cos^2 \Theta_{ij} - 1) (3I_{zi}I_{zj} - \mathbf{I}_i \cdot \mathbf{I}_j) \quad (2)$$

where \mathbf{I} and I_z are spin angular momentum operators, γ is the gyromagnetic ratio of the spins, r_{ij} is the distance between spins i and j , and Θ_{ij} is the angle between the internuclear vector \mathbf{r}_{ij} and the applied magnetic field.

Rapid molecular motion results in a motionally averaged Hamiltonian

$$\langle \mathcal{H}_D^{ij} \rangle = -\frac{\gamma^2 \hbar}{2\pi} \left\langle \frac{1}{2r_{ij}^3} (3 \cos^2 \Theta_{ij} - 1) \right\rangle (3I_{zi}I_{zj} - \mathbf{I}_i \cdot \mathbf{I}_j) \quad (3)$$

where the angle brackets $\langle \rangle$ indicate an average over all

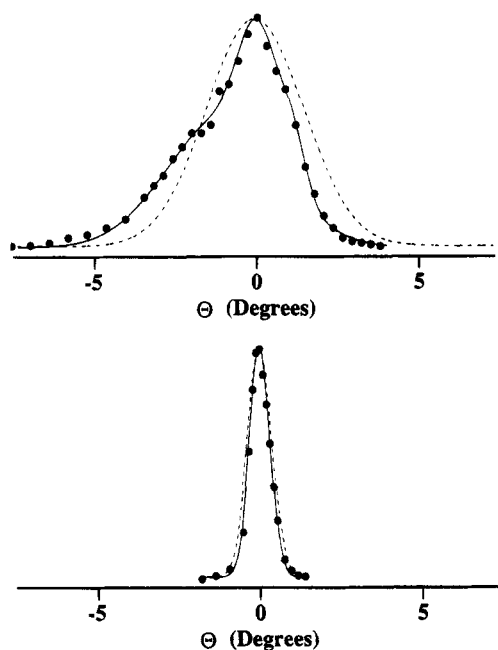


Figure 6. Mosaic spread of the graphite layers in $\text{Cs}(\text{THF})_{1.3}\text{C}_{24}$ (top) and $\text{K}(\text{THF})_{2.5}\text{C}_{24}$ (bottom) as measured by X-ray diffraction. With the detector set to verify the Bragg condition corresponding to the (002) reflection, the intensity as a function of sample orientation is a direct measure of the orientational distribution of the graphite layers in the sample. The solid circles represent experimental points, the solid lines represent Gaussian fits, and the dashed lines are the distributions used in the simulations of the experimental spectra.

molecular conformations and orientations. As shown in the Appendix, if the mosaic spread of the sample is neglected, the expression of the motionally averaged factor of the dipolar Hamiltonian is given by

$$\left\langle \frac{1}{2r_{ij}^3} (3 \cos^2 \Theta_{ij} - 1) \right\rangle = \frac{1}{2} (3 \cos^2 \Theta - 1) \left\langle \frac{1}{2r_{ij}^3} (3 \cos^2 \theta_{ij}^k - 1) \right\rangle \quad (4)$$

where θ_{ij}^k is the angle between the internuclear vector \mathbf{r}_{ij} and the crystallite \mathbf{c}_k axis.

The resolution of the room-temperature spectra of the Cs/THF and K/THF GICs in Figures 4 and 5 suggests that intermolecular dipole couplings are essentially averaged to zero, and only the intramolecular couplings remain. Thus, to a good approximation, the room-temperature NMR spectra can be considered to result from isolated, eight-spin THF molecules, which can be simulated numerically. The spectrum of an eight-spin system with C_{2v} symmetry (possibly the symmetry of the time-averaged THF molecule) still has up to 2860 lines, leading to a crowded spectrum with extensive overlap of lines. Nevertheless, the spectra of THF in the highly oriented GICs studied here exhibit enough resolution and characteristic features to permit analysis.

In addition to the dipole couplings, the chemical shifts of the protons on THF could play a role in determining the shape of the NMR spectra. The measured spectra are almost symmetric at all sample orientations, showing that the chemical shift difference between the α and β protons of THF is small compared to the dipole couplings. For our simulations we used a chemical shift difference of 200 Hz (2 ppm), which is approximately the difference in the measured isotropic chemical shift values.^{21,22}

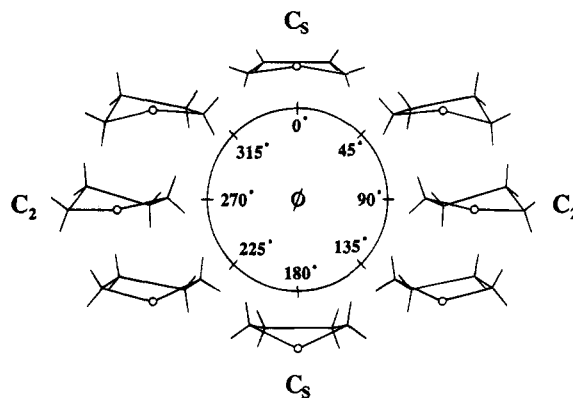


Figure 7. Conformations of THF as a function of the pseudorotation angle ϕ . The conformers at $\phi = 0^\circ$ and 180° have C_s symmetry, and the conformers at $\phi = 90^\circ$ and 270° have C_2 symmetry.

4.2. THF Motion. To simulate the spectra of THF, the motional average in eq 4 must be carried out over the molecular motions of THF in the GIC. Possible motions include molecular rotation and conformational changes. THF, like other five-membered-ring molecules, is not planar but is puckered and displays an internal motion known as pseudorotation, shown in Figure 7. Pseudorotation is a vibrational mode originally postulated for cyclopentane¹⁸ and subsequently observed for THF²³ and other molecules.²⁴ To describe the different pseudorotation conformations, we use the model by Kilpatrick et al.¹⁸ improved by Geise et al.²⁵ From this model, the coordinates of the oxygen and carbon atoms in THF are calculated as a function of two parameters, q and ϕ , which characterize the ring puckering. The distance of a ring atom from the molecular mean plane is given by

$$z(i) = \sqrt{\frac{2}{5}} q \cos\left(\frac{4\pi}{5}i + \phi\right) \quad (5)$$

where i labels the ring atoms from 0 (oxygen) to 4. The in-plane atomic coordinates are calculated according to the additional constraint that the atoms move along a strongly curved trajectory defined to minimize the variation in C–C and C–O bond lengths with changes in phase and amplitude of the puckering. The proton coordinates are calculated by assuming a fixed C–H bond length (1.115 Å) and H–C–H angle (109.47°). Each H–C–H plane is perpendicular to the plane defined by the carbon atom and its two nearest heavy atom neighbors, and the intersection of both planes bisects the H–C–H angle. The geometrical parameters used to obtain the proton coordinates as a function of q and ϕ are given in ref 25.

Previous studies^{26–28} have shown that pseudorotation in THF is not free as in cyclopentane but can be parametrized using a potential of the form

$$V(\phi) = V_2 \cos(2\phi) + V_4 \cos(4\phi) \quad (6)$$

where V_2 and V_4 are constants and ϕ is the phase of the pseudorotation.

In addition to pseudorotation, the anisotropic rotation of THF molecules as a whole must be included in the simulations. With respect to the crystallite reference frame (Oz parallel to the crystallite \mathbf{c}_k axis), the molecular frame (Oz_m perpendicular to the mean plane, the Ox_mOz_m plane containing the oxygen atom) is rotating about \mathbf{c}_k . The orientation of the crystallite frame with respect to the molecular frame can be characterized by two angles: α , the angle of rotation of the molecular frame about Oz_m , and β , the angle between \mathbf{c}_k and Oz_m , as shown in Figure 8.

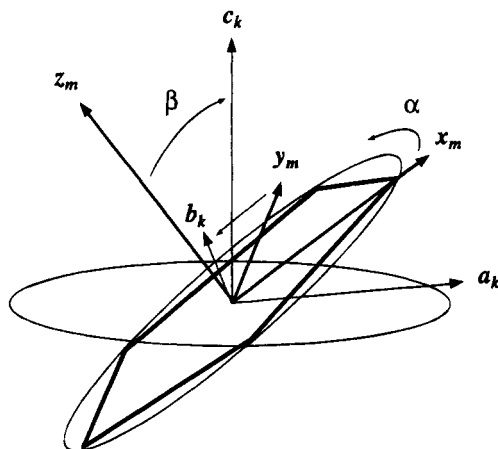


Figure 8. Definition of Euler angles (α, β) relating the molecular frame (x_m, y_m, z_m) to the crystallite frame (a_k, b_k, c_k). To rotate the molecular frame into the crystallite frame, it is first rotated about z_m by α then about b_k by β .

The simulations of the proton NMR spectra of THF in K/THF and Cs/THF GICs were performed using computer programs written by the authors in the laboratory of Professor Pines at the University of California, Berkeley. The pseudorotation amplitude q , the coefficients V_2 and V_4 of the pseudorotation potential, and the orientation of the THF molecules within the intercalated layers (defined by the angles α and β) were adjusted to minimize the difference between the experimental and simulated spectra. The quality of the fit of a simulated spectrum to the experimental spectrum for a given set of adjustable parameters was determined by visual comparison of the spectra. The uncertainty in each adjustable parameter gives a measure of the size of the change in each parameter that is required to produce a noticeable difference in the simulated spectrum. The mosaic spread of crystallite orientation in each sample was modeled by introducing a Gaussian distribution of orientations for the rotation axes (Figure 6).

5. Results

5.1. Cs(THF)_{1.3}C₂₄. Previous studies of Cs/THF GICs^{12,19} concluded that due to steric constraints imposed by the small I_c of 7.1 Å, the THF molecules must have their mean planes parallel to the graphite layers. This is confirmed by our simulations where only the orientation $\beta = 0^\circ$ of the THF molecules within intercalated layers gives simulated spectra with an overall width greater than 80 kHz, as in the experimental spectra. Any other orientation gives simulated spectra that are too narrow, implying that the THF molecules must have their mean planes parallel to the graphite layers, as inferred from the qualitative analysis in section 3.1.

With the mean plane of THF parallel to the graphite layers and rotation of the THF molecules about an axis perpendicular to the graphite layers, the simulated spectrum of the $\Theta = 0^\circ$ orientation of the Cs(THF)_{1.3}C₂₄ GIC was optimized with respect to the parameters q , the ring puckering amplitude, and V_2 and V_4 , the constants in the pseudorotation potential of eq 6. The best fit to the experimental data was obtained with $q = 0.30 \pm 0.01$ Å, $V_2 = -15 \pm 5$ kJ/mol, and $V_4 = 3 \pm 2$ kJ/mol and is shown in Figure 9. The value of q is somewhat less than that found for gaseous THF of 0.38–0.44 Å^{23,25,29} and that found for THF in a liquid crystal of 0.39 Å.²⁸ The values found for V_2 and V_4 do not correspond to hindered pseudorotation but instead to interconversion between two conformations at $\phi = 0^\circ$ and 180° with a barrier of 30 kJ/mol between them, giving a probability distribution that is significantly different from zero only for $\phi = 0 \pm 20^\circ$ and $180 \pm 20^\circ$.

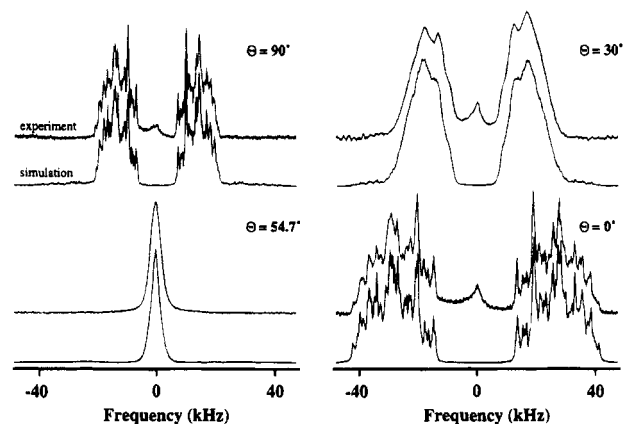


Figure 9. Simulations (bottom) of the experimental spectra (top) of Cs(THF)_{1.3}C₂₄ for several values of Θ , the angle between the external magnetic field and the normal to the graphite layers. The simulations were carried out with the mean planes of the THF molecules parallel to the graphite layers and the molecules rotating about an axis perpendicular to the layers. The parameters $q = 0.30$ Å, $V_2 = -15$ kJ/mol, $V_4 = 3$ kJ/mol, and line broadening of 200 Hz were used, and appropriately weighted spectra of different orientations were added together to simulate the mosaic spread of the layers in Figure 6.

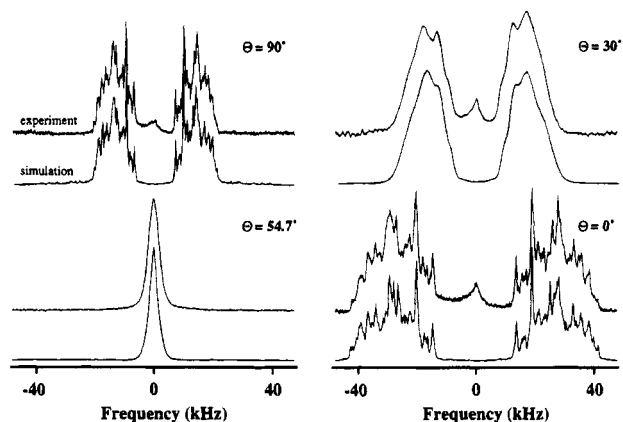


Figure 10. Simulations of the spectra of Cs(THF)_{1.3}C₂₄ as in Figure 9, except with only one conformation, $\phi = 0^\circ$, and with $q = 0.32$ Å.

One other good fit to the experimental data was obtained with THF fixed in one conformation, $\phi = 0^\circ$. In this case, it was found that the experimental spectra could be most accurately simulated with $q = 0.32 \pm 0.01$ Å, as shown in Figure 10.

5.2. K(THF)_{2.5}C₂₄. The first attempts to simulate the spectra of K(THF)_{2.5}C₂₄ indicated that the THF molecules cannot have their mean planes perpendicular to the graphite layers but must have some orientation intermediate between perpendicular and parallel. Varying the orientation of the THF molecules in addition to their conformation would introduce two more adjustable parameters. Therefore, some simplifying assumptions had to be made in our further simulations. Since the line shape appears to be more sensitive to changes in the orientation than to the details of the molecular conformation, the values of q , V_2 , and V_4 were no longer varied, but rather taken from the best simulations of the Cs(THF)_{1.3}C₂₄ compound. Only the orientation of the THF molecules was allowed to vary.

The best fit to the experimental spectra for the case of two conformations of THF ($q = 0.30$ Å, $V_2 = -15$ kJ/mol, and $V_4 = 3$ kJ/mol) was obtained by averaging over orientations of THF defined by the Euler angles $\alpha = 40^\circ$ – 120° and $\beta = 71^\circ$ and is shown in Figure 11. In this simulation the THF molecules have their mean planes tilted slightly away from perpendicular to the graphene layers, and oscillate about an axis perpendicular

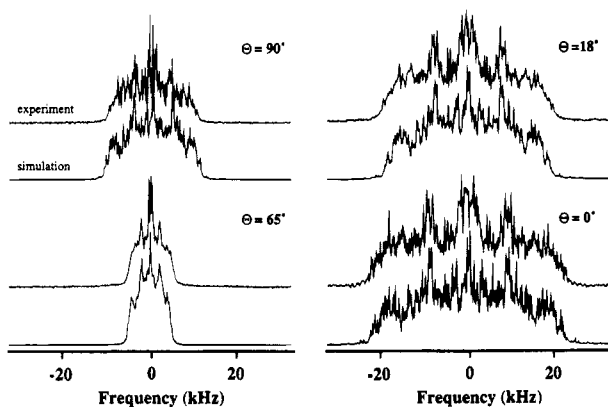


Figure 11. Simulations (bottom) of the experimental spectra (top) of $\text{K}(\text{THF})_{2.5}\text{C}_{24}$ for several Θ , the angle between the external magnetic field and the normal to the graphite layers. The values of Θ in this figure are the values used in the simulations and can be compared to the experimental values in Figure 5. The simulations were carried out by averaging over orientations of THF molecules defined by the Euler angles $\alpha = 40^\circ$ through 120° and $\beta = 71^\circ$ as defined in the text. The values $q = 0.30 \text{ \AA}$, $V_2 = -15 \text{ kJ/mol}$, $V_4 = 3 \text{ kJ/mol}$, and line broadening of 100 Hz were used.

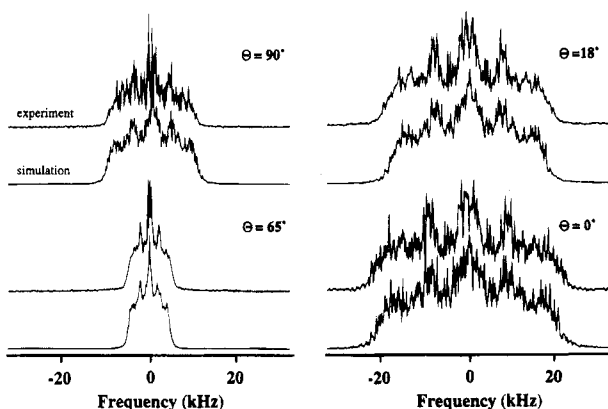


Figure 12. Simulations of spectra of $\text{K}(\text{THF})_{2.5}\text{C}_{24}$ as in Figure 11, but with a fixed THF conformation of $\phi = 0^\circ$ and a fixed orientation of the THF molecules defined by the Euler angles $\alpha = 22^\circ$ and $\beta = 55^\circ$.

to the rings' mean planes, moving the oxygen atoms through a range of angles which keep it away from the graphene layers.

The simulations with only one conformation ($\phi = 0^\circ$ and $q = 0.32 \text{ \AA}$) gave a best fit to the experimental spectra for THF oriented at Euler angles of $\alpha = 22^\circ$ and $\beta = 55^\circ$, shown in Figure 12. In this case the mean plane of THF is tilted further away from the layer normal, with the oxygen atoms oriented approximately toward the layers. Additional motions, besides rotation about an axis perpendicular to the graphite layers, are possible but cannot be discerned from our simulations.

6. Discussion

The experimental spectra of $\text{Cs}(\text{THF})_{1.3}\text{C}_{24}$ are satisfactorily simulated by two different sets of parameters, describing either one conformation C_s ($\phi = 0^\circ$ and $q = 0.32 \text{ \AA}$) or the interconversion between two C_s conformations ($q = 0.30 \text{ \AA}$, $\phi = 0^\circ$ and 180°). The second hypothesis seems more likely since the thermal evolution of the ^1H line shape below 273 K displays a slight increase in the second moment at about 200 K ,¹⁴ indicating that the THF molecules are not completely frozen when the molecular reorientation ceases.

Previous studies of saturated K/THF GICs^{7,30} have concluded from the larger interlayer spacing of 8.9 \AA that the mean planes of the THF molecules are approximately perpendicular to the

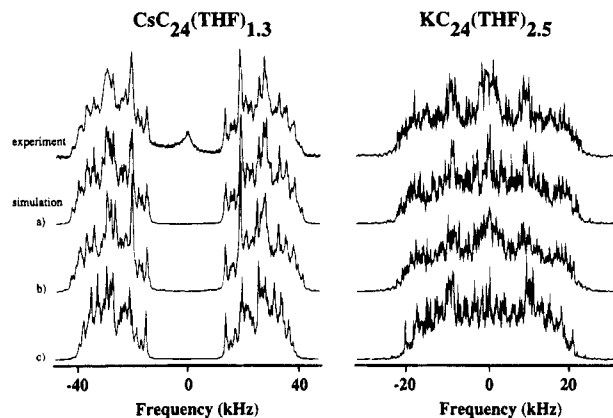


Figure 13. Simulations of the spectra of $\text{Cs}(\text{THF})_{1.3}\text{C}_{24}$ and $\text{K}(\text{THF})_{2.5}\text{C}_{24}$ at angle $\Theta = 0^\circ$ with free pseudorotation (simulation c) compared with simulations assuming two conformations as in Figures 9 and 11 (simulation a) or one fixed conformation as in Figures 10 and 12 (simulation b).

graphite layers. Though experimental data are not reproduced as well as for the Cs/THF sample, the results from our simulations show that the THF molecules cannot be perpendicular to the graphite layers but have their mean planes oriented between 15° and 40° from perpendicular to the graphite layers. Similar to Cs/THF GICs, the thermal evolution of the ^1H line width of a K/THF GIC powder sample below room temperature¹¹ shows that the THF molecules are still moving at temperatures below 150 K . Consequently, conformational mobility superimposed on the anisotropic reorientation at room temperature appears very likely, and simulations with parameters involving only one conformation are not credible.

The values of q , V_2 , and V_4 found to describe the conformational mobility and puckering amplitude of THF in $\text{Cs}(\text{THF})_{1.3}\text{C}_{24}$ are different from the ones used to describe THF in the gaseous state or in the liquid state. Greenhouse et al.²⁶ and Engerholm et al.²⁷ found values of $V_2 = 0.16 \text{ kJ/mol}$ and $V_4 = 0.24 \text{ kJ/mol}$ for gaseous THF, corresponding to slightly hindered pseudorotation. Esteban et al.²⁸ were unable to determine unique values for V_2 and V_4 for THF dissolved in a nematic liquid crystal but concluded that their data were most consistent with nearly free pseudorotation. These differences are the result of the constrained environment imposed by the graphite layers. The graphite matrix and the interaction with the metal cations appear to deform the THF molecules slightly from their equilibrium conformation as well as to prevent them from pseudorotating.

The conformational mobility of THF in the K/THF compound was described with the same parameters q , V_2 , and V_4 as used for the Cs/THF compound. This assumption may not be valid, since the temperature at which the THF molecules are completely frozen is not the same in the two compounds. It appears, however, that the simulations of the spectra of $\text{K}(\text{THF})_{2.5}\text{C}_{24}$ are much more sensitive to the orientation of the THF molecules than to their conformation, so it may be impossible to gain any insight into the conformation of THF in this compound from the ^1H NMR spectra. In fact, while simulations of the ^1H spectra of C/THF GIC with free pseudorotation ($V_2 = V_4 = 0$ in eq 6) reproduce the experimental data rather poorly (Figure 13), the situation is not so clear for the K/THF compound. None of the simulations of this compound—with two conformations (Figure 11), with one conformation (Figure 12) and with free pseudorotation (Figure 13)—are sufficiently good to rule out the others. Further simulations varying the THF orientational parameters α and β together with the conformational ones q ,

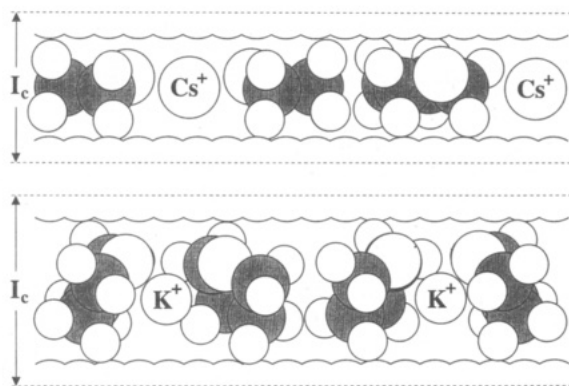


Figure 14. Schematic pictures of $\text{Cs}(\text{THF})_{1.3}\text{C}_{24}$ and $\text{K}(\text{THF})_{2.5}\text{C}_{24}$ that are consistent with the results of the simulations of the proton NMR spectra. The values of I_c determined by X-ray diffraction are 7.1 \AA for $\text{Cs}(\text{THF})_{1.3}\text{C}_{24}$ and 8.9 \AA for $\text{K}(\text{THF})_{2.5}\text{C}_{24}$.

V_2 , and V_4 would be more easily done with deuterium or multiple-quantum ^1H spectra.

7. Conclusion

Proton NMR spectra of molecules in graphite intercalation compounds can provide detailed information about these molecules. Simulations of the ^1H NMR spectra of $\text{Cs}(\text{THF})_{1.3}\text{C}_{24}$ and $\text{K}(\text{THF})_{2.5}\text{C}_{24}$ provide information about the conformation, orientation, and motion of the THF molecules in these compounds.

Simulations of the ^1H NMR spectra of $\text{Cs}(\text{THF})_{1.3}\text{C}_{24}$ confirm previous observations that the THF molecules in this compound are oriented with their mean planes parallel to the graphite layers and are rotating about an axis perpendicular to the layers. Additionally, the simulations show that conformational mobility of THF in this compound is strongly reduced compared to the nearly free pseudorotation observed for THF in the gas or liquid phase. Interconversion between the two C_s conformations of THF with pseudorotation angles $\phi = 0^\circ$ and $\phi = 180^\circ$ is the only internal motion that produces simulated spectra that match the experimental spectra.

Simulations of the ^1H NMR spectra of the K/THF GIC are not as conclusive, but they do indicate that the THF molecules in this compound are oriented with their mean planes oriented between 50° and 75° from parallel to the graphite layers, balanced between the forces from the graphite layers above and below and from neighboring THF molecules and K^+ ions on the sides. Conformational motion of THF in the K/THF GIC cannot be determined.

From this work emerges a picture of the Cs/THF and K/THF GICs like that shown in Figure 14. Further studies using deuterium or multiple-quantum NMR could provide more information about the nature of the motion occurring in these compounds.

Acknowledgment. We thank F. Béguin for the preparation of the GIC compounds and help with the X-ray measurements. C.S. acknowledges financial support by the Alexander von Humboldt Foundation. M.E.R. was supported by a National Science Foundation Graduate Fellowship. This work was supported by the Director, Office of Energy Research, Office of Basic Energy Sciences, Materials Sciences Division of the U.S. Department of Energy under Contract DE-AC03-76SF00098.

Appendix

In this appendix, extensive use is made of rotational transformations between reference frames using Euler angles and Wigner rotation matrices. Euler angles (α, β, γ) correspond

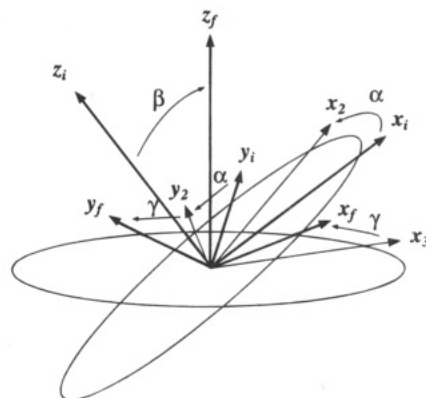


Figure 15. Definition of Euler angles (α, β, γ) used to rotate one frame into another. To rotate an initial frame (x_i, y_i, z_i) into a final frame (x_f, y_f, z_f) , first rotate the initial frame by α about z_i to (x_2, y_2, z_2) , then rotate by β about y_2 to (x_3, y_3, z_3) , then rotate by γ about z_f to (x_f, y_f, z_f) .

to successive rotations about rotated axes, as defined in Figure 15. The Euler angles required to rotate an initial frame (Ox, Oy, Oz) into a final frame (OX, OY, OZ) are (α, β, γ) where (α, β) are the polar angles of OZ in the initial frame and γ is a rotation about the new OZ axis. Wigner matrix elements $\mathcal{D}_{m,n}^{(2)}(\alpha, \beta, \gamma)$ and reduced Wigner matrix elements $d_{m,n}^{(2)}(\beta)$ are defined by

$$\mathcal{D}_{m,n}^{(2)}(\alpha, \beta, \gamma) = \langle 2m | e^{-i\alpha J_x} e^{-i\beta J_y} e^{-i\gamma J_z} | 2n \rangle = e^{-im\alpha} d_{m,n}^{(2)}(\beta) e^{-iny}$$

and

$$d_{m,n}^{(2)}(\beta) = \langle 2m | e^{-i\beta J_y} | 2n \rangle$$

where J_x , J_y , and J_z are the appropriate projections of the angular momentum, and $|2m\rangle$, $|2n\rangle$, are eigenstates of \mathbf{J}^2 and J_z . Expressions for reduced matrix elements can be found in ref 31. A rotation $\mathcal{D}_{m,n}^{(2)}(\alpha, \beta, \gamma)$ can also be expressed as a series of two successive rotations $(\alpha_1, \beta_1, \gamma_1)$ followed by $(\alpha_2, \beta_2, \gamma_2)$ ³¹

$$\mathcal{D}_{m,n}^{(2)}(\alpha, \beta, \gamma) = \sum_{p=-2}^{+2} \mathcal{D}_{m,p}^{(2)}(\alpha_1, \beta_1, \gamma_1) \mathcal{D}_{p,n}^{(2)}(\alpha_2, \beta_2, \gamma_2) \quad (\text{A-1})$$

Since the GIC samples used in this study are polycrystalline, a crystallite frame labeled by the index k is introduced. In this frame, the \mathbf{c}_k axis (perpendicular to the graphite planes) and the in-plane crystallographic \mathbf{a}_k axis are chosen as Oz_k and Ox_k axes, respectively. With the successive frame changes defined by the Euler angles

$$\begin{array}{ccc} \text{proton-proton frame} & \xrightarrow{(\alpha_{ij}^k, \beta_{ij}^k, \gamma_{ij}^k)} & \\ & & \text{crystallite frame} \xrightarrow{(\alpha_k, \beta_k, \gamma_k)} \\ & & \text{laboratory frame} \end{array}$$

the motionally averaged factor $\langle (1/r_{ij}^3)(3 \cos^2 \Theta_{ij} - 1) \rangle$ in eq 3 can be rewritten ($\beta_{ij} = \Theta_{ij}$)

$$\left\langle \frac{1}{r_{ij}^3} \mathcal{D}_{0,0}^{(2)}(\alpha_{ij}, \beta_{ij}, \gamma_{ij}) \right\rangle = \sum_{q=-2}^2 \left\langle \frac{1}{r_{ij}^3} \mathcal{D}_{0,q}^{(2)}(\alpha_{ij}^k, \beta_{ij}^k, \gamma_{ij}^k) \right\rangle \mathcal{D}_{q,0}^{(2)}(\alpha_k, \beta_k, \gamma_k) \quad (\text{A-2})$$

Based on the crystallographic structure of HOPG samples, the crystallite \mathbf{c}_k axis orientation throughout the sample is very close to the sample \mathbf{c} axis. Therefore, with $\beta_k = \beta + \delta\beta_k$, to first

order in $\delta\beta_k$, the Wigner matrix elements $\mathcal{D}_{q,0}^{(2)}(\alpha_k, \beta_k, \gamma_k)$ can be written

$$\mathcal{D}_{q,0}^{(2)}(\alpha_k, \beta_k, \gamma_k) \approx e^{-iq\alpha_k} \left[d_{q,0}^{(2)}(\beta) + \delta\beta_k \left(\frac{d}{d\theta} d_{q,0}^{(2)}(\theta) \right)_{\theta=\beta} \right] \quad (\text{A-3})$$

The averaged term in eq A-2, assuming an axially symmetric motion, can be rewritten in terms of a symmetry axis frame labeled sa. As above, we define the following Euler angles

$$\begin{array}{ccc} \text{proton pair frame} & \xrightarrow{(\alpha_{ij}^{\text{sa}}, \beta_{ij}^{\text{sa}}, \gamma_{ij}^{\text{sa}})} & \\ & \text{symmetry axis frame} \xrightarrow{(\alpha_{sa}^k, \beta_{sa}^k, \gamma_{sa}^k)} & \\ & & \text{crystallite frame} \end{array}$$

Using eq A-1, the averaged terms in eq A-2 are rewritten as

$$\left\langle \frac{1}{r_{ij}^3} \mathcal{D}_{0,q}^{(2)}(\alpha_{ij}^k, \beta_{ij}^k, \gamma_{ij}^k) \right\rangle = \sum_{q=-2}^2 \left\langle \frac{1}{r_{ij}^3} \mathcal{D}_{0,q}^{(2)}(\alpha_{ij}^{\text{sa}}, \beta_{ij}^{\text{sa}}, \gamma_{ij}^{\text{sa}}) \right\rangle \mathcal{D}_{q,q}^{(2)}(\alpha_{sa}^k, \beta_{sa}^k, \gamma_{sa}^k) \quad (\text{A-4})$$

Due to the axial symmetry of the motion, eq A-4 is invariant under a rotation through γ_{ij}^{sa} about Oz^{sa} . In this case, eq A-4 is valid only when $q' = 0$ and reduces to

$$\left\langle \frac{1}{r_{ij}^3} \mathcal{D}_{0,q}^{(2)}(\alpha_{ij}^k, \beta_{ij}^k, \gamma_{ij}^k) \right\rangle = \left\langle \frac{1}{r_{ij}^3} \mathcal{D}_{0,0}^{(2)}(\alpha_{ij}^{\text{sa}}, \beta_{ij}^{\text{sa}}, \gamma_{ij}^{\text{sa}}) \right\rangle d_{0,q}^{(2)}(\beta_{sa}^k) e^{-iq\gamma_{sa}^k} \quad (\text{A-5})$$

Combining eqs A-2, A-3, and A-5, we can write

$$\left\langle \frac{1}{r_{ij}^3} \mathcal{D}_{0,0}^{(2)}(\alpha_{ij}^k, \beta_{ij}^k, \gamma_{ij}^k) \right\rangle \approx \left\langle \frac{1}{r_{ij}^3} \mathcal{D}_{0,0}^{(2)}(\alpha_{ij}^{\text{sa}}, \beta_{ij}^{\text{sa}}, \gamma_{ij}^{\text{sa}}) \right\rangle \mathcal{F}^{k,\text{sa}}(\beta) \quad (\text{A-6})$$

where $\mathcal{F}^{k,\text{sa}}(\beta)$ is defined as

$$\mathcal{F}^{k,\text{sa}}(\beta) = \sum_{q=-2}^2 \left[d_{q,0}^{(2)}(\beta) + \delta\beta_k \left(\frac{d}{d\theta} d_{q,0}^{(2)}(\theta) \right)_{\theta=\beta} \right] e^{-iq(\alpha_k + \gamma_{sa}^k)} d_{0,q}^{(2)}(\beta_{sa}^k) \quad (\text{A-6}')$$

The dependence of $\langle \mathcal{K}_{ij}^i \rangle$ on the orientation of the sample with respect to the magnetic field is therefore contained in the function $\mathcal{F}^{k,\text{sa}}(\beta)$, which depends on the crystallite orientation through $(\alpha_k, \delta\beta_k)$ and the symmetry axis through $(\beta_{sa}^k, \gamma_{sa}^k)$.

The ratio $|\mathcal{F}^{k,\text{sa}}(90^\circ)/\mathcal{F}^{k,\text{sa}}(0^\circ)|$ is of special interest because from the experimental spectra, its value is expected to be $1/2$ (see section 3). From the explicit form of $d_{q,0}^{(2)}(\beta)$ and $d_{0,q}^{(2)}(\beta_{sa}^k)$, we obtain, to zeroth order in $\delta\beta_k$

$$\left| \frac{\mathcal{F}^{k,\text{sa}}(90^\circ)}{\mathcal{F}^{k,\text{sa}}(0^\circ)} \right| = \left| -\frac{1}{2} + \frac{3}{2} \frac{\sin^2 \beta_{sa}^k}{3 \cos^2 \beta_{sa}^k - 1} \cos(\alpha_k + \gamma_{sa}^k) \right| \quad (\text{A-7})$$

Equation A-7 shows that this ratio is independent of the crystallite orientation only if $\sin^2 \beta_{sa}^k$ vanishes. In that case, the ratio $|\mathcal{F}^{k,\text{sa}}(90^\circ)/\mathcal{F}^{k,\text{sa}}(0^\circ)|$ takes the value $1/2$, and the

function $\mathcal{F}^{k,\text{sa}}(\beta)$ reduces to

$$\mathcal{F}^{k,\text{sa}}(\beta) = \frac{1}{2}(3 \cos^2 \beta - 1) - \frac{3}{2} \delta\beta_k \sin 2\beta$$

To zeroth order in $\delta\beta_k$, this leads to eq 4 in section 4. In this equation, the polar angles of \mathbf{r}_{ij} refer to the crystallite frame because the symmetry axis Oz^{sa} is parallel to the crystallite c_k axis.

References and Notes

- (1) Abragam, A. *The Principles of Nuclear Magnetism*; Clarendon: Oxford, 1961; Chapter 10.
- (2) *Nuclear Magnetic Resonance of Liquid Crystals*; Emsley, J. W., Ed.; NATO ASI Series C; D. Reidel Publishing: Dordrecht, 1985; Vol. 141.
- (3) Zabel, H.; Solin, S. A. *Graphite Intercalation Compounds I. Structure and Dynamics*; Springer Series in Materials Science; Springer-Verlag: Berlin, 1990.
- (4) Zabel, H.; Solin, S. A. *Graphite Intercalation Compounds II. Transport and Electronic Properties*; Springer Series in Materials Science; Springer-Verlag: Berlin 1992.
- (5) Solin, S. A.; Zabel, H. *Adv. Phys.* **1988**, *37*, 87.
- (6) Panich, A. M. *J. Magn. Reson.* **1986**, *66*, 9.
- (7) Facchini, L.; Quinton, M.-F.; Legrand, A. P.; Béguin, F.; Setton, R. *Physica B* **1980**, *99*, 525.
- (8) Miller, G. R.; Moran, M. J.; Resing, H. A.; Tsang, T. *Langmuir* **1986**, *2*, 194.
- (9) Kunoff, E. M.; Goren, S. D.; Korn, C.; Riesenmeier, H.; Stang, I.; Lüders, K. *Phys. Rev. B* **1989**, *39*, 6148.
- (10) Béguin, F.; Gonzalez, B.; Conard, J.; Estrade-Szwarckopf, H.; Guérard, D. *Synth. Met.* **1985**, *12*, 187.
- (11) Quinton, M.-F.; Legrand, A. P.; Béguin, F. *Synth. Met.* **1986**, *14*, 179.
- (12) Goldmann, M.; Dianoux, A. J.; Gonzalez, B.; Béguin, F.; Szwarckopf, H. Estrade; Conard, J. *Synth. Met.* **1988**, *23*, 55.
- (13) Béguin, F.; Guérard, D.; Goldmann, M. *Synth. Met.* **1989**, *34*, 33.
- (14) Béguin, F.; Laroche, C.; Gonzalez, B.; Goldmann, M.; Quinton, M.-F. *Synth. Met.* **1988**, *23*, 155.
- (15) Laane, J. In *Vibrational Spectra and Structures*; Durig, J. R., Ed.; Dekker: New York, 1972; pp 25–50.
- (16) Fuchs, B. In *Topics in Stereochemistry*; Allinger, N. L., Eliel, E. L., Eds.; J. Wiley: New York, 1978; pp 1–94.
- (17) Legon, A. C. *Chem. Rev.* **1980**, *80*, 231.
- (18) Kilpatrick, J. E.; Pitzer, K. S.; Spitzer, R. *J. Am. Chem. Soc.* **1947**, *69*, 2483.
- (19) Goldmann, M.; Pannetier, J.; Béguin, F.; Gonzalez, B. *Synth. Met.* **1988**, *23*, 133.
- (20) Fukushima, E.; Roeder, S. B. W. *Experimental Pulse NMR*; Addison-Wiley: Reading, MA, 1981; Chapter 2, pp 92–97.
- (21) Diez, E.; Esteban, A. L.; Rico, M. *J. Magn. Reson.* **1974**, *16*, 136.
- (22) Lozach, R.; Lemarie, B.; Braillon, B. *J. Chim. Phys.* **1975**, *72*, 873.
- (23) Lafferty, W. J.; Robinson, D. W.; St. Louis, R. V.; Russell, J. W.; Strauss, H. L. *J. Chem. Phys.* **1965**, *42*, 2915.
- (24) Pitzer, K. S.; Donath, W. E. *J. Am. Chem. Soc.* **1959**, *81*, 3213.
- (25) Geise, H. J.; Adams, W. J.; Bartell, L. S. *Tetrahedron* **1969**, *25*, 3045.
- (26) Greenhouse, J. A.; Strauss, H. L. *J. Chem. Phys.* **1969**, *50*, 124.
- (27) Engerholm, G. G.; Luntz, A. C.; Gwinn, W. D.; Harris, D. O. *J. Chem. Phys.* **1969**, *50*, 2446.
- (28) Esteban, A. L.; Galache, M. P.; Diez, E.; San Fabian, J.; Bermejo, F. *J. Mol. Phys.* **1990**, *69*, 429.
- (29) Davidson, R.; Warsop, P. A. *J. Chem. Soc., Faraday Trans. 2* **1972**, *68*, 1875.
- (30) Béguin, F.; Setton, R.; Hamwi, A.; Touzain, P. *Mater. Sci. Eng.* **1979**, *40*, 167.
- (31) Mehring, M. *Principles of High Resolution NMR in Solids*, 2nd ed.; Springer-Verlag: Berlin, 1983; pp 292–295. Note that $d_{2,2}^{(2)} = d_{-2,-2}^{(2)}$, and not $= d_{-2,2}^{(2)}$, as misprinted in this book.

JP942534Q